Optimization Methods of MPPT Parameters for PV Systems: Review, Classification, and Comparison

Jalal Dadkhah and Mehdi Niroomand

***Abstract*—To obtain efficient photovoltaic (PV) systems, optimum maximum power point tracking (MPPT) algorithms are inevitable. The efficiency of MPPT algorithms depends on two MPPT parameters, i. e., perturbation amplitude and perturbation period. The optimization of MPPT algorithms affect both the tracking speed and steady-state oscillation. In this paper, optimization methods of MPPT parameters are reviewed and classified into fixed and variable methods. The fixed MPPT parameters are constant during MPPT performance, and a trade-off should be made between the tracking speed and steady-state oscillation. However, the variable MPPT parameters will be changed to improve both the tracking speed and the steady-state oscillations. Moreover, some of them are simulated, compared, and discussed to evaluate the real contributions of the optimization methods to the MPPT efficiency. Furthermore, significant features of the optimization methods, i.e., noise immunity, robustness, and computation effort, are investigated.**

***Index Terms*—Photovoltaic (PV) systems, maximum power point tracking (MPPT), perturbation amplitude, perturbation period.**

I. Introduction

PHOTOVOLTAIC (PV) systems have recently gained popularity since they are environmentally friendly and can be installed in residential and remote areas. In PV systems, the output power reaches the maximum at a point called maximum power point (MPP), and its location continuously changes based on the irradiance level and temperature. As a result, to extract the maximum power from the PV generator (PVG), an operation point should be located at MPP. Therefore, MPP must continuously be tracked by maximum power point tracking (MPPT) algorithms. Generally, MPPT algorithms are classified into two categories due to uniform irradiance and partial shading conditions [1]. Perturb and observe (P&O) [2] and incremental conductance (INC) [3] algorithms are examples of the first category. Particle swarm optimization (PSO) [4] and hybrid techniques [5] are applied under partial shading conditions to find the global MPP.

MPPT algorithms are usually applied in either single-loop or multi-loop MPPT structures. In the single-loop MPPT structure, the MPPT algorithm directly changes the duty cycle D of interfacing power converter (IPC), as shown in Fig. 1(a). However, the input voltage controller (IVC) adjusts the duty cycle in the multi-loop MPPT structure, as shown in Fig. 1(b) [6]. v_{pv} and v_o are the small-signal parts of the PV voltage and power output to load, respectively.

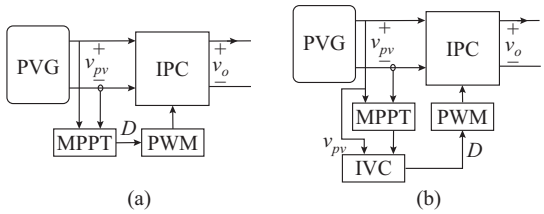

Fig. 1. Different PV system structures. (a) Single-loop. (b) Multi-loop.

The efficiency of MPPT highly depends on the MPPT parameters, i.e., perturbation amplitude ΔD and perturbation period T_p. The perturbation amplitude is a change either to the duty cycle of IPC in the single-loop structure or to the reference voltage ΔV_{ref} and reference current ΔI_{ref} in the multi-loop structure. The perturbation period is the time interval between two consecutive perturbations. The characteristics of the MPPT perturbation which lead to the optimum efficiency of MPPT is depicted in Fig. 2, in which the MPPT perturbation has the amplitude of $2\Delta D$ and the period of $4T_p$ [7].

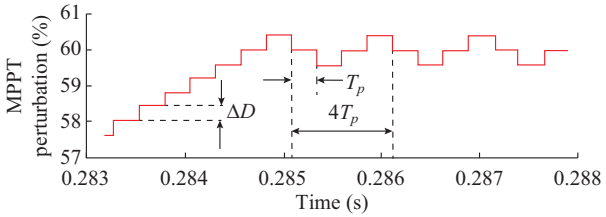

Fig. 2. ΔD and T_p on duty cycle of IPC leading to optimum efficiency of MPPT.

In the literature, different types of MPPT algorithms are studied ranging from the conventional algorithms to smart

Manuscript received: June 8, 2019; accepted: April 23, 2020. Date of Cross-Check: April 23, 2020. Date of online publication: January 25, 2021.

J. Dadkhah is with the Department of Electrical Engineering, University of Isfahan, Isfahan, Iran, and he is also with the Department of Electrical and Computer Engineering, University of Manitoba, Winnipeg, Canada (e-mail: dadkhahj@myumanitoba.ca).

M. Niroomand (corresponding author) is with the Department of Electrical Engineering, University of Isfahan, Isfahan, Iran (e-mail: mehdi_niroomand@eng.ui.ac.ir).

DOI: 10.35833/MPCE.2019.000379

ones [8]. In this paper, the optimization methods of MPPT parameters have been studied and classified into fixed and variable methods. Moreover, the small-signal analysis of PV systems is provided to make a clear background about the dynamic behavior of PV systems, which is necessary for the optimization of the MPPT parameters. Furthermore, different values of the MPPT parameters are compared to show how they affect the PV system efficiency. Finally, some of the surveyed methods are simulated under the same simulation conditions to make a fair comparison among different methods. As a result, interesting facts have been revealed such as why steady and transient states need different optimization methods, how much optimization methods contribute to the efficiency of MPPT, and how some optimization methods can be fused together to increase their robustness.

II. Analysis of Small-signal Model of PV Systems

A. Dynamic and Static Resistors of PV Panels

According to Fig. 3, the *I-V* curve of a PV panel consists of two distinct regions, i. e., the constant current region (CCR) and the constant voltage region (CVR), which are separated by MPP [9]. Because of the finite accuracy of digital microcontrollers, the operation point can never be located at MPP and oscillates around MPP. Therefore, another region is formed around MPP called the constant power region (CPR). Consequently, dynamic resistor r_{pv} and static resistor R_{pv} are defined for a PV panel based on (1) and (2), respectively.

$$r_{pv} \approx -v_{pv}/i_{pv} \tag{1}$$

$$R_{pv} = V_{pv}/I_{pv} \tag{2}$$

where V_{pv} and I_{pv} are the DC parts of the PV voltage and the PV current, respectively.

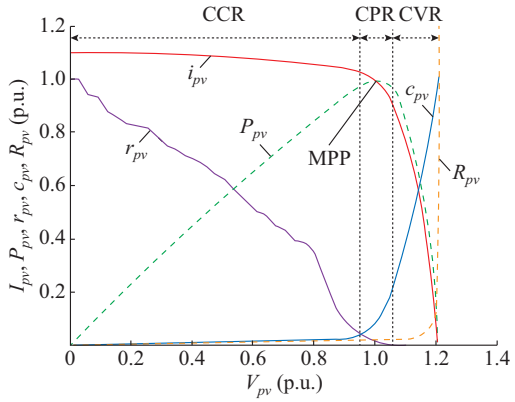

Fig. 3. *I-V* and *P-V* curves of dynamic and static resistors.

According to Fig. 3, r_{pv} is the maximum at the short-circuit current, the minimum at the open-circuit voltage, and equal to R_{pv} at MPP. In the structure of the single-loop MPPT, r_{pv} affects the parameters of PV system such as the damping factor ξ_{pv} and the settling time T_ε. In fact, r_{pv} has an inverse relation with ξ_{pv} and direct relation with T_ε. Therefore, the single-loop PV system has the maximum T_ε at the short-circuit current and the minimum T_ε at the open-circuit voltage. On the contrary, in the case of the multi-loop MPPT structure, the impact of the dynamic resistor on T_ε is negligible.

B. PV System Modeling

The PV system shown in Fig. 4 can be modeled by the duty cycle to the PV voltage transfer function G_{ci}^{pv} in the single-loop MPPT structure.

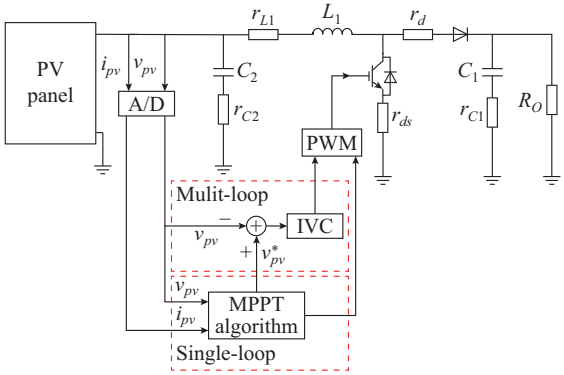

Fig. 4. PV system consisting of a PV panel, a boost converter, and a resistive load.

Therefore, the PV voltage dynamic characteristics can be derived by (3) and (4) in response to the perturbation ΔD [9].

$$\begin{cases} G_{ci}^{pv}(s) = -V_{DC}\dfrac{\omega_n^2(1+s/\omega_{z,esr})}{s^2+2\xi_{pv}\omega_n s+\omega_n^2} \\ \omega_n \approx \sqrt{1/(L_1 C_2)} \\ \omega_{z,esr} = 1/(r_{C2} C_2) \\ \xi_{pv} \approx 0.5\left(\dfrac{1}{r_{pv}}\sqrt{L_1/C_2}+R_e\sqrt{C_2/L_1}\right) \\ R_e = r_{L1}+r_{C2}+Dr_{ds}+(1-D)r_d \end{cases} \tag{3}$$

where ω_n is the natural frequency; $\omega_{z,esr}$ is the zero frequency induced by the input capacitor equivalent series resistance; ξ_{pv} is the damping factor; V_{DC} is the DC gain; and C_1, C_2, L_1, r_{C1}, r_{C2}, r_{L1}, r_d, and r_{ds} are the circuit parameters of Fig. 4.

The response of the PV voltage to ΔD as in (4) can be calculated by (3). Consequently, by substituting (4) into (5)-(7), the PV power response in different regions can be achieved [9]. Note that (5) is in CCR, (6) is in CVR, and (7) is in CPR.

$$\begin{cases} \hat{v}_{pv}(s) = \hat{d}G_{ci}^{pv} = -V_{DC}\Delta D\left(\dfrac{1}{s}-\dfrac{s+2\xi_{pv}\omega_n-\dfrac{\omega_n^2}{\omega_{z,esr}}}{s^2+2\xi_{pv}\omega_n s+\omega_n^2}\right) \\ \hat{d}(s) = \dfrac{\Delta D}{s} \end{cases} \tag{4}$$

$$\hat{P}_{pv} \approx I_{pv}\hat{v}_{pv}r_{pv} \gg R_{pv} \tag{5}$$

$$\hat{P}_{pv} \approx -(v_{pv}/r_{pv})\hat{v}_{pv}r_{pv} \ll R_{pv} \tag{6}$$

$$\hat{P}_{pv} \approx -(1/R_{pv})\hat{v}_{pv}^2 r_{pv} \approx R_{pv} \tag{7}$$

Moreover, when the MPPT structure is multi-loop, (8) can be derived by the reference voltage $\hat{v}_{pv}^*$ to the PV voltage transfer function $T(s)$ [6].

$$T(s)=\frac{\hat{v}_{pv}}{\hat{v}_{pv}^{*}}=\frac{C(s)P(s)}{1+C(s)P(s)} \tag{8}$$

where $P(s)=\hat{v}_{pv}/\hat{d}$ is the open-loop PV voltage loop plant and $C(s)$ is the transfer function of the IVC. By substituting (8) into (9)-(11), the PV power for the multi-loop structure can be achieved in different regions [6]. Note that (9) is in CCR, (10) is in CVR, and (11) is in CPR.

$$\hat{P}_{pv}\approx I_{pv}L^{-1}(\hat{v}_{pv}^{*}(s)T(s)) \tag{9}$$

$$\hat{P}_{pv}\approx -(v_{pv}/r_{pv})L^{-1}(\hat{v}_{pv}^{*}(s)T(s)) \tag{10}$$

$$\hat{P}_{pv}\approx -(1/R_{pv})(L^{-1}(\hat{v}_{pv}^{*}(s)T(s)))^{2} \tag{11}$$

where $L^{-1}(\cdot)$ is the inverse Laplace transform operator. Finally, the parameters of PV system performance such as the PV power settling time in both the single-loop and multi-loop structures can be achieved in different regions by (5)-(7) and (9)-(11), respectively.

III. Effects of ΔD and T_p on Efficiency of PV System

In this section, different values of MPPT parameters are compared to show how they affect the efficiency of PV system. The single-loop PV system in Fig. 4 is simulated in MATLAB/Simulink software based on the values of $L_1=550$ μH, $C_1=C_2=150$ μF, $r_{C1}=r_{C2}=10$ mΩ, $r_{L1}=0.1$ Ω, $r_{ds}=44$ mΩ, $r_d=0$, $R_O=15$ Ω, switching frequency $f_{sw}=60$ kHz, 120 W PV panel, and P&O MPPT algorithm. Afterwards, observations from the simulations are justified by an analytical expression to assess how the MPPT parameters affect the efficiency of PV system.

A. Effects of ΔD

The perturbation amplitude is a change which is applied by MPPT algorithm to the duty cycle of IPC. According to Fig. 5, the small value of ΔD decreases steady-state oscillations while the large value of ΔD increases steady-state oscillations.

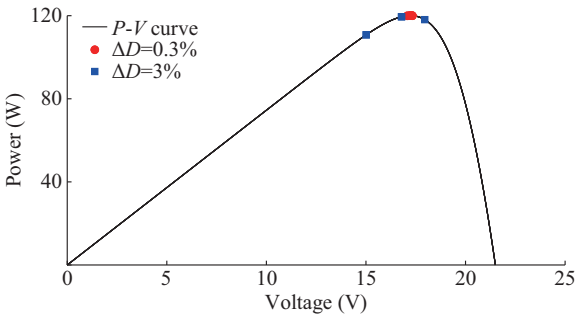

Fig. 5. Effect of ΔD on oscillation amplitude of operation point around MPP.

B. Effects of T_p

The optimum value of T_p leads to the three-point oscillation in the steady state. According to Fig. 6, the values of T_p which are smaller than the system settling time increase both the amplitude and number of oscillations around MPP. According to Fig. 7, the value of T_p which is greater than the system settling time maintains three-point oscillation.

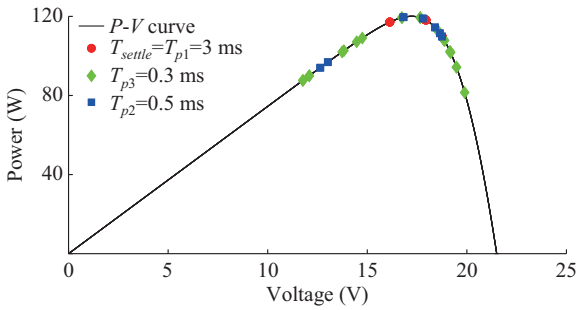

Fig. 6. Effect of T_p which is smaller than system settling time on oscillation amplitude of operation point around MPP.

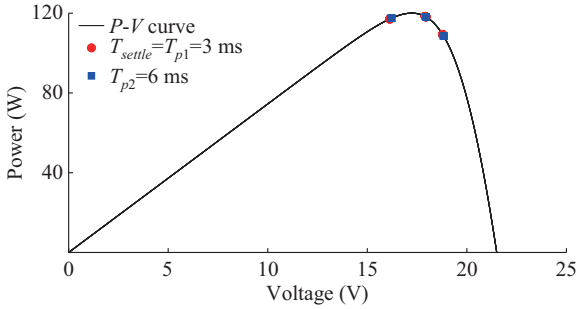

Fig. 7. Effect of T_p which is greater than system settling time on oscillation amplitude of operation point around MPP.

The steady-state efficiency described by (12) shows how the above observations affect the PV system efficiency.

$$\eta_{MPPT}=1-\frac{\alpha\Delta V^{2}\left(N_R^{2}+N_L^{2}+2\sum_{k=1}^{N_R-1}k^{2}+2\sum_{j=1}^{N_L-1}j^{2}\right)}{2(N_L+N_R)P_{MPP}} \tag{12}$$

where N_L and N_R are the numbers of oscillation points in the left and right sides of MPP, respectively [10]; α is a constant; ΔV is the PV voltage difference; and P_{MPP} is the maximum power [10]. When N_L and N_R increase as shown in Fig. 6, the second term in (12) increases. Consequently, the efficiency of MPPT decreases.

IV. Optimization Methods of ΔD

The proper selection of ΔD leads to fast and accurate tracking of MPP. Therefore, the knowledge of optimization methods of ΔD is of importance to reach high efficiency in PV systems. According to Fig. 8, the optimization methods of ΔD are classified into fixed and variable methods.

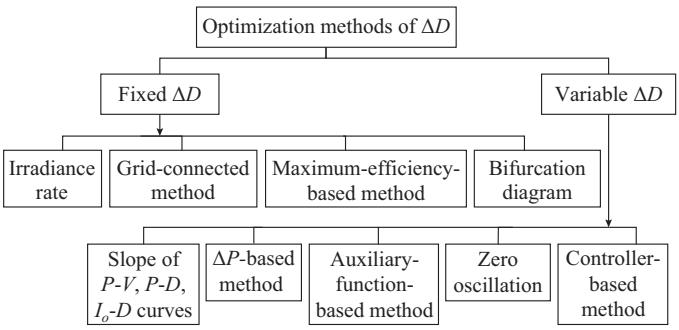

Fig. 8. Optimization methods of perturbation amplitude.

A. Fixed ΔD

In the fixed Δ*D* methods, Δ*D* is calculated in the design stage and is constant during the MPPT performance. Large Δ*D* shortens the transient time while it increases oscillation amplitude in the steady state. Small Δ*D* extends the transient time while it decreases oscillation amplitude in the steady state. Therefore, a trade-off should be made between the transient speed and the steady-state efficiency.

1) Irradiance Rate

The main idea of this kind of method is to select Δ*D* (13) in a way that the MPPT algorithm can distinguish the variations of the PV power caused by the duty cycle modulation from those caused by the irradiance variation. As a result, the MPPT algorithm does not fail to track MPP when the irradiance level changes with the rate of $\dot{G}$ [6], [7], [10].

$$\Delta D > \frac{1}{|G_0|}\sqrt{\frac{V_{MPP}K_{ph}|\dot{G}|T_p}{HV_{MPP}+\frac{1}{r_{pv}}}} \tag{13}$$

where G_0 is the DC gain of (3); V_{MPP} is the PV voltage at MPP; $\dot{G}$ is the rate of the irradiance change; and K_{ph} and H are the parameters.

2) Grid-connected PV System

In grid-connected PV systems shown in Fig. 9 [7], the bulk capacitor introduces another perturbation which leads to the malfunction of the MPPT algorithm [11]. In fact, the MPPT algorithm is not able to distinguish the variations of the PV voltage caused by the duty cycle modulation from those caused by the grid. This problem will be solved if Δ*D* is selected by (14) [7].

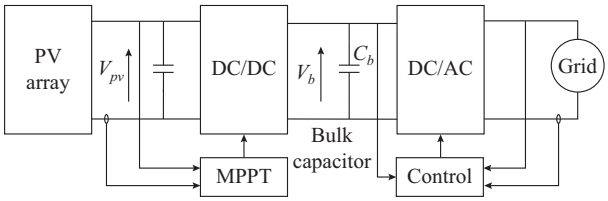

Fig. 9. Dual-stage grid-connected PV system.

$$\Delta D > \frac{1}{|G_0|}\sqrt{\frac{V_{MPP}K_{ph}|\dot{G}|T_p}{HV_{MPP}+\frac{1}{r_{pv}}}}+\frac{1-D}{|G_0|}\frac{P_{MPP}}{2\pi f_{ac}C_bV_b} \tag{14}$$

where C_b, V_b, and f_{ac} are the bulk capacitor, the voltage across C_b, and the grid frequency, respectively.

3) Maximum-efficiency-based Method

Achieving the maximum efficiency is a desire for all the mentioned methods. It is directly used in the form of a formula. For instance, the maximum efficiency which is a function of ΔV_{ref} is given by (15). With different values of ΔV_{ref}, the optimum one that leads to the highest efficiency can be achieved [12].

$$\eta=\frac{2P_{MPP}+V_{MPP}i_{d,0}\left(1-\frac{q\Delta V_{ref}}{kAT}\cos h\right)-\Delta V_{ref}i_{d,0}\frac{q\Delta V_{ref}}{kAT}\sin h}{2P_{MPP}} \tag{15}$$

where $i_{d,0}$ is the current through the *p-n* junction of a PV cell; q is the electron charge, $q=160\times10^{-21}$; k is Boltzmann's constant, $k=13.8\times10^{-24}$; A is the diode quality factor; and T is the absolute temperature. According to Fig. 10, another example of this method is described in (16), which is derived based on the difference of power between MPP (point *A*) and point *B*. Therefore, by solving (16), the optimum value of Δ*D* is derived [13].

$$v_{mpp}i_{mpp}(1-\beta)=i_{pv,B}(v_{mpp}+\Delta DV_B) \tag{16}$$

where β is the maximum admissible loss; and $i_{pv,B}$ and V_B are the current and voltage of point *B*, respectively.

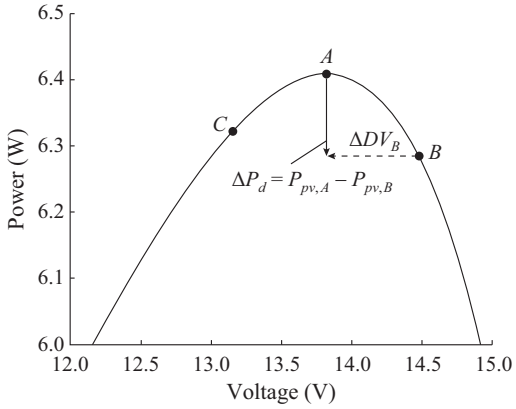

Fig. 10. Choosing optimum Δ*D* based on power difference between point *A* and point *B*.

4) Bifurcation Diagram

A bifurcation diagram shows the effect of a bifurcation parameter on the system performance and can be used to determine the appropriate range of the parameter in the design stage. Therefore, this diagram is used to determine a proper Δ*D*. According to Fig. 11, the PV voltage will have the best performance if Δ*D* is selected between 0.02% and 0.07% [2], [3].

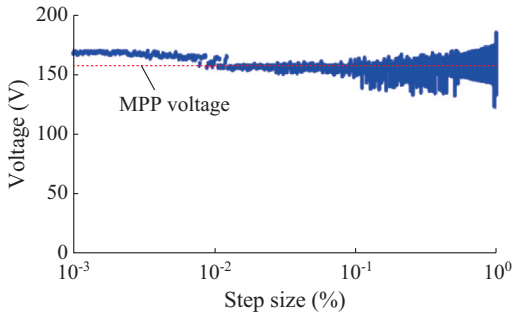

Fig. 11. Bifurcation diagram of PV voltage-step size for P&O algorithm.

B. Variable ΔD

Variable Δ*D* has been proposed to improve not only the steady-state behavior but also the dynamic performance of MPPT algorithms. Several important methods are introduced as follows.

1) Slope of P-V, P-D, and I_o-D Curves

In some special curves such as *P-V*, *P-D*, and I_o-*D*, the slope has an increasing trend. In fact, according to Fig. 12,

the slope gradually increases from MPP to the extreme left and right sides [14]-[18]. Therefore, based on (17), the slope of these curves can be used to determine ΔD. However, selecting an appropriate scaling factor N is the main difficulty for such methods.

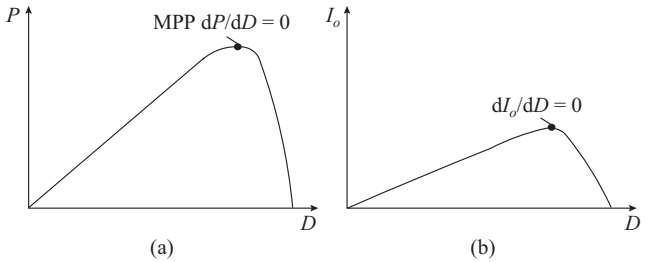

Fig. 12. P-D and I_o-D curves. (a) P-D curve. (b) I_o-D curve.

$$\begin{cases} \Delta D = N\left|\Delta P/\Delta V\right| \\ N < \left|\Delta D_{\max}/\Delta P/\Delta V\right|_{\Delta D_{\max}} \end{cases} \tag{17}$$

where N is the scaling factor; $\Delta D_{\max}$ is the fixed maximum perturbation amplitude; and ΔP and ΔV are the differences in the PV power and voltage between two consecutive samples, respectively.

2) ΔP-based Method

In the previous method, a small value of ΔV leads to a large value of ΔD, thus the operation point moves away from MPP. In addition, it needs a division operation. Therefore, one possible solution to address the problem is to use only the difference in ΔP (18) [19], [20].

$$\Delta D = N_2\left|\Delta P\right| \tag{18}$$

where N_2 is the scaling factor.

3) Auxiliary-functions-based Method

Auxiliary functions are mostly derived from the P-V and P-D curves and are used to determine variable ΔD or the area in which MPP is located. In fact, in some methods, the limit of MPP is firstly predicted either by simple methods like fractional open-circuit voltage [21] or by advanced methods like Lambert function [22] and the function in Fig. 13 [23], [24].

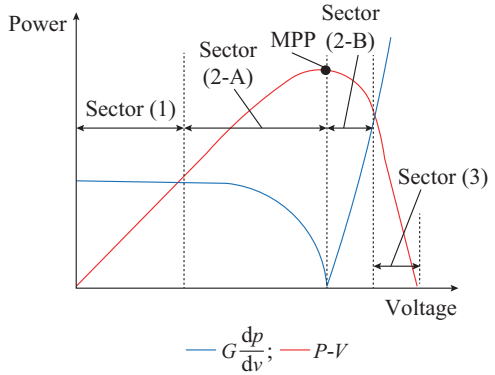

Fig. 13. Auxiliary function used for predicting limit of MPP.

Afterwards, based on the location of the operation point than the predicted area, small and big values are assigned to ΔD, seperately. Auxiliary functions are used to determine the variable ΔD. However, according to Fig. 14, there are cases in which variable ΔD is determined by auxiliary functions without predicting the area of MPP [25]-[30]. In Fig. 14, e^B is the exponential function

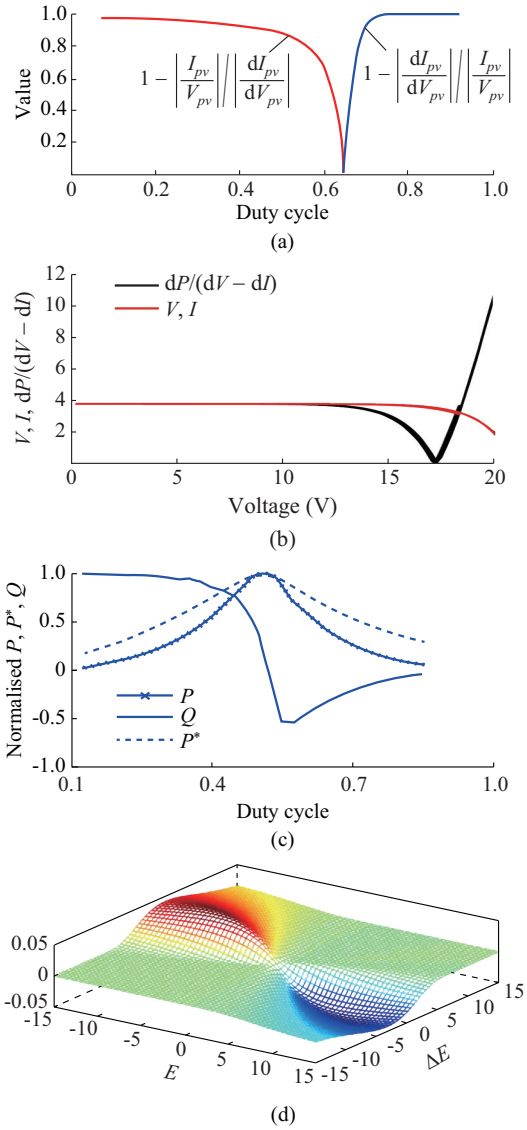

Fig. 14. Auxiliary functions used for determining variable ΔD. (a) $F = 1-\left|dI_{pv}/dV_{pv}\right|\Big/\left|I_{pv}/V_{pv}\right|$ and $G = 1-\left|I_{pv}/V_{pv}\right|\Big/\left|dI_{pv}/dV_{pv}\right|$. (b) $V, I, dP/(dV-dI)$. (c) $P, P^*, Q = (1-D)dV_{pv} + V_{pv}dD$. (d) $\Delta D = A\tan^{-1}((E-\Delta E)/\gamma)e^B$.

For example, the variable ΔD is determined by the two curves in Fig. 14(a), in which their values are either nearly zero when the operation point is near MPP or nearly one when the operation point is far from MPP. The curve in Fig. 14(b) has the same behavior as that in Fig. 14(a) although the right-side slope is greater than the left-side one as shown in Fig. 14(b). Figure 14(c) shows three curves in which P and P^* are used to derive the final curve Q which determines both the variable ΔD and its sign. Furthermore, the function in Fig. 14(d) constituting of a two-dimensional Gaussian function and Arctangent function generates both variable ΔD and its sign. However, its performance highly

depends on the argument parameters of the Gaussian function.

4) Zero Oscillation

In this method, the steady state is firstly identified either by the recognition of the three-point oscillation around MPP [31]-[36] or by the number of operation point movements around MPP [37]. Afterwards, ΔD is selected equal to zero or gradually decreases in the steady state. Therefore, the steady-state oscillations are completely or partially removed. However, the three-point oscillation will be guaranteed if T_p is optimized. Otherwise, these methods will not work efficiently. Moreover, in the case of zero oscillation, the PV voltage and current have to be continuously checked whether there are changes that stem from the variation of weather conditions or not.

5) Controller-based Method

According to Fig. 15, ΔP can be treated as an error signal for digital controllers to produce variable ΔD [38]-[41]. For instance, proportional-integral controller tuned by Zigler-Nicholas method [39] and proportional-integral-derivative (PID) controller tuned by the genetic algorithm (GA) [38] are used to produce variable ΔD. The main contributions of these methods are to reduce oscillations around MPP and to improve the dynamic response of PV systems under fast-changing environmental conditions.

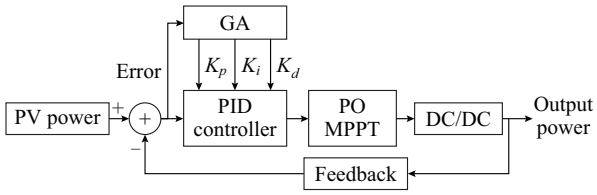

Fig. 15. Block diagram of controller-based method.

V. Optimization Methods of T_p

The optimized value of T_p leads to the three-point oscillation in the steady state and the fast tracking in the transient state. Therefore, the knowledge of the optimization methods of T_p is of vital importance to improve the efficiency of MPPT. According to Fig. 16, the optimization methods of T_p are classified into fixed and variable methods.

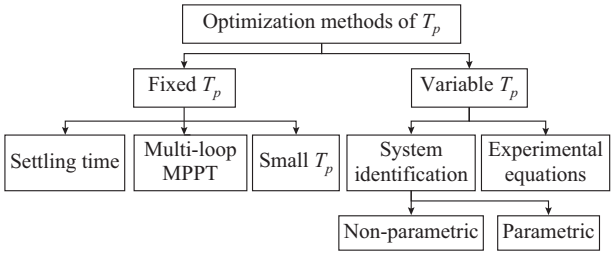

Fig. 16. Optimization methods of perturbation period.

A. Fixed T_p

In this method, T_p is calculated in the design stage and is constant with MPPT performance. Large T_p extends the transient time while it guarantees the three-point oscillation in the steady state. On the contrary, small T_p leads to the fast tracking while it increases oscillations around MPP to more than three points.

1) Settling Time

By setting T_p to be the settling time of PV system, MPPT waits enough before applying the next perturbation so that the fluctuation of the PV voltage and current is restricted to a band of $\pm\varepsilon$. Therefore, the sampled PV voltage and current lead to the correct tracking of MPP. The settling time of PV system can either be calculated in CPR by (19) [7], [30], [35] or measured experimentally [42]-[44].

$$\begin{cases} T_\varepsilon \cong -\dfrac{1}{\xi_{pv}\omega_n}\ln(\varepsilon) \\ \varepsilon = 0.1 \end{cases} \tag{19}$$

where ε is the relative magnitude of settling band. Furthermore, it is proven that the settling time of PV system in CCR (20) is longer than CPR and CVR [9]. Thus, the settling time in CCR can provide a safer value for T_p. Moreover, ξ_{pv} in CCR is easy to calculate since it only depends on IPC parameters. Moreover, ξ_{pv} in CPR and CVR depends not only on IPC parameters but also on r_{pv} which is tricky to be determined.

$$T_p = -\frac{1}{\xi_{pv}\omega_n}\ln\left(\varepsilon\sqrt{1-\xi_{pv}^2}\right) \tag{20}$$

2) Multi-loop MPPT

When the MPPT structure is multi-loop, the effect of the PV panel dynamic resistor on the system settling time is negligible [6]. Therefore, the optimization of T_p in the multi-loop MPPT structure is different from that in the single-loop one. For instance, when IVC is the integral controller or PID controller, (21) and (22) are used to determine the system settling time, respectively.

$$T_\varepsilon = \frac{1}{G\bar{G}^{-1}\omega_c}\ln\left(\frac{2}{\varepsilon}\right) \tag{21}$$

$$T_\varepsilon \approx \frac{1}{\xi_a\omega_a}\ln\left(\frac{1}{\varepsilon\sqrt{1-\xi_a^2}}\right) \tag{22}$$

where G, $\bar{G}$, and ω_c are the DC gain of $P(s)$ in (8), the nominal value of G, and a desired loop gain crossover frequency, respectively; ξ_a is the damping factor; and ω_a is the natural frequency.

3) Small T_p

When T_p is equal to the IPC switching period or the digital-to-analog conversion period, the tracking speed substantially increases [2], [3]. In this case, the system is not locally stable since the system waveforms are irregular and non-periodic. However, as the system waveforms are limited between the two levels, the system is globally stable. Therefore, when the MPPT structure is multi-loop, the loss of local stability may result in instability of IVC and malfunction of the MPPT algorithm. Thus, this method only works for the single-loop MPPT structure.

B. Variable T_p

The settling time of PV system is affected by environmental factors, system components, and ΔD. Therefore, fixed T_p cannot be a valid value under different weather conditions.

Thus, system identification techniques and experimental equations have been applied to provide an adaptive T_p for PV systems.

1) System Identification

System identification techniques are used to identify important parameters of system performance which can be used for system monitoring or controller tuning. System identification techniques are classified into two categories: non-parametric and parametric [45]. Non-parametric techniques do not need any system model and only need a proper exciting signal such as a pseudo random binary sequence (PRBS) [46], [47]. However, parametric techniques are based on a plant model [48].

Recently, the system identification techniques have been used in PV systems to identify the online value of T_p. According to (19), ξ_{pv} and ω_n determine the settling time and the value of T_p. However, ξ_{pv} and ω_n depend on r_{pv}, weather conditions, and IPC parameters. Furthermore, the aging phenomenon of PV systems affects the values of ξ_{pv} and ω_n. As a result, with the online system identification, the optimized value of T_p can be achieved independent of PV system component values, weather conditions, and the aging phenomenon.

1) Non-parametric

According to Fig. 17 [10], the identification procedure is started as soon as the steady state is reached. Afterwards, the MPPT function is halted, and PRBS is injected to the duty cycle of IPC. The impulse response $h(n)$ of the PV system is achieved by cross-correlating the PV voltage and the PRBS, and the frequency response $G_{vp,d}(k)$ of the PV system is derived by applying fast Fourier transform (FFT) to $h(n)$. Finally, the online value of T_p is calculated from the identified frequency response [10], [49].

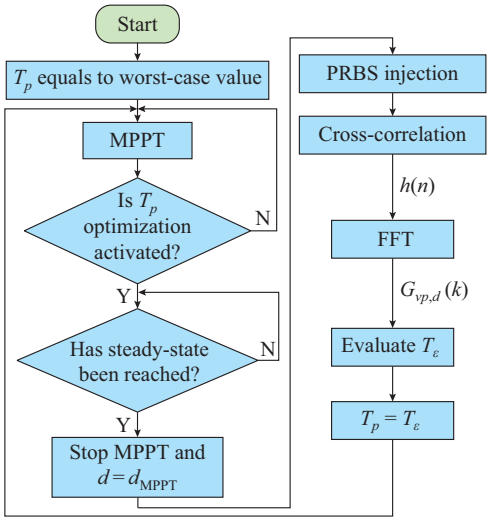

Fig. 17. Flowchart of non-parametric system identification of PV system.

2) Parametric

The overall procedure in the parametric system identification is similar to the non-parametric one. Nevertheless, the objective of the parametric system identification is to identify the parameters of the defined PV system model. The Kalman filter [50], [51] and dichotomous coordinate descent-recursive least squares (DCD-RLS) method are used [52]. The Kalman filter needs numerous initializations. However, zero is assumed as the initial value in DCD-RLS method, which has better identification speed and accuracy.

2) Experimental Equations

In this method, an experimental equation which is a function of ΔD is derived to determine T_p. In fact, different values of ΔD lead to different values of the settling time. Therefore, according to Fig. 18 [16], the settling time is measured for different values of ΔD, and the measured data is estimated by a linear function (23) [16], [29]. However, this method is only efficient for the transient state. In fact, when the irradiance level changes and the PV system reaches a new steady state, the settling time also changes. As a result, T_p in the steady state is obtained from (24), in which PV current is proportional to the irradiance level [53].

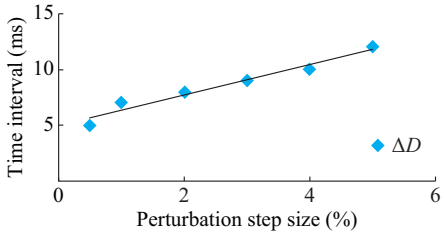

Fig. 18. Settling time of PV system versus ΔD.

$$T_p = f\left(|\Delta D|\right) = 1.3644|\Delta D| + 4.9753 \tag{23}$$

$$T_p = 0.00903\exp\left(-0.218\, I_{PV}\right) \tag{24}$$

VI. Discussion and Comparison

The contribution of the mentioned optimization methods to the PV system efficiency is quantified by conducting simulations in MATLAB/Simulink software. Afterwards, simulation results are compared and discussed. Since the methods are simulated under the same simulation condition and selected from different mentioned categories, it is possible to draw a fair comparison. To this end, the PV system in Fig. 4 is used. Electrical parameters of Fig. 4 are described in Table I.

TABLE I
Electrical Parameters of Boost Converter and PV Panel

Device	Parameter	Value
Boost converter	C_1=C_2	150 μF
	L_1	550 μF
	H	10 mΩ
	r_{C1}=r_{C2}	0.1 Ω
	r_{L1}	44 mΩ
	r_{ds}	0
	R_O	15 Ω
	f_{sw}	60 kHz
PV panel	P_{max}	120 W
	V_{MPP}	16.9 V
	I_{MPP}	7.1 A
	V_{OC}	21.5 V
	I_{SC}	7.45 A

The simulation results are given in Table II and Figs. 19-22. In fact, MPPT parameters are shown in Figs. 20 and 22, in which the transient and steady states are labeled with *T-S* and *S-S*, respectively. Their corresponding output power and voltage are depicted in Figs. 19 and 21. Furthermore, in Table II, the tracking speed is T_{rising} when the irradiance goes up from 500 W/m^2 to 1000 W/m^2 and $T_{falling}$ when the irradiance goes down from 1000 W/m^2 to 500 W/m^2. T_{rising} and $T_{falling}$ are decided when the output power reaches 95% of its final value. In addition, the efficiency of MPPT is calculated by (25) [27]. The fixed T_p is equal to 8.5 ms, which is the settling time of PV system under the worst condition with the lowest irradiance level. Moreover, the computation effort of each method is mentioned in Table II. It is decided based on the number of pre-tuned parameters, linear and non-linear functions, and the number of code lines.

$$\eta_{MPPT}=\frac{\int_0^t P_{pv}(t)\mathrm{d}t}{\int_0^t P_{mpp}(t)\mathrm{d}t}\times 100\% \tag{25}$$

where P_{mpp} is the theoretical maximum power.

The importance of ΔD on the efficiency of MPPT is revealed in Table II. In fact, when ΔD goes up from 2% to 3.5%, the transient state speeds up by 50% approximately. When the steady-state oscillation increases, the considerable improvement of the transient state leads to the increase of the efficiency of MPPT by 3%. Moreover, the bifurcation diagram along with small T_p achieves the fastest tracking speed about 10 ms with the merit of computation simplicity. However, the method has disadvantages of steady-state oscillations due to small T_p, susceptibility to the noise due to the small ΔD and local instability as discussed in the Section V.

The method of variable ΔD further improves the efficiency of MPPT although the results are not desirable in some cases. For instance, according to methods No. 4 and No. 5 of Table II, the optimized ΔD has a smooth decreasing behavior in the first and the second transient states. Nevertheless, they are not effective in the third transient state for the duration of around 100 ms. Simulation results are presented in Figs. 19 and 20. In fact, *P-V* curve has different slopes in the right and left sides of MPP while the scaling factor in (17) is tuned based on one side. Therefore, either T_{rising} or $T_{falling}$ improves. Despite this deficiency, method No. 4 produces 2% energy more than $\Delta D=3.5\%$. Concerning the issue of the scaling factor, ΔD in Fig. 20(h) is optimized by two scaling factors tailored for each side of MPP, thus the tracking speed reaches around 30 ms according to Fig. 19(h).

TABLE II
SIMULATION RESULTS OF REVIEWED METHODS

No.	Optimization method	MPPT algorithm	ΔD	T_p (ms)	Tracking speed (ms)		η_{MPPT} (%)	Computation effort
					T_{rising}	$T_{falling}$		
1	Irradiancerate [7]	P&O	Fixed, 2.0%	Fixed, 8.500	115	86	90.2	Simple
2	Maximum efficiency [12]	P&O	Fixed, 3.5%	Fixed, 8.500	73	45	93.1	Simple
3	Bifurcation diagram + small T_p [2]	P&O	Fixed, 0.08%	Fixed, 0.016	5	10	98.0	Simple
4	Slope of *P-V* curve [18]	P&O	Variable, Fig. 20(b)	Fixed, 8.500	64	103	95.1	Moderate
5	Auxiliary function [26]	INC	Variable, Fig. 20(c)	Fixed, 8.500	90	86	93.9	Moderate
6	Based on ΔP [19]	P&O	Variable, Fig. 20(d)	Fixed, 8.500	244	53	81.1	Simple
7	Auxiliary function [21]	CSAM[a]	Variable, Fig. 20(e)	Fixed, 8.500	31	35	94.8	Moderate
8	Zero oscillation [35]	ASF-Beta[b]	Variable, Fig. 20(f)	Fixed, 8.500	47	43	98.0	Moderate
9	Auxiliary functions + experimental equations [29]	GAF-VPF[c]	Variable, Fig. 20(g)	Variable, Fig. 22(b)	73	90	93.9	Moderate
10	System identification [10]	P&O	Fixed, 2.5%	Variable, Fig. 22(c)	74	37	95.8	Complex
11	Auxiliary functions + experimental equations [53]	P&O	Variable, Fig. 20(h)	Variable, Fig. 22(d)	27	34	96.3	Moderate

Note: a indicates current sensorless method with Auto-Modulation; b indicates adaptive scaling factor Beta method; c indicates Gaussian-Arctangent function based on variable perturbation frequency.

Method No. 6, which indicates the optimized ΔD based on ΔP, is computationally simple. Moreover, it is not efficient since the first steady state is missed according to Figs. 19(d) and 20(d). Thus, it has the lowest efficiency of 81.1%.

Furthermore, method No. 7 speeds up the transient states at the cost of wild fluctuations in the steady states according to Figs. 19(e) and 20(e). Also, its performance highly depends on pre-tuned parameters, thus it has no robustness under different weather conditions. According to Figs. 19(f) and 20(f), method No. 8 that has zero oscillation in the steady states reaches as the highest efficiency as in method No. 3 while method No. 8 has much lower tracking speed than that in method No. 3. The reason is that the zero oscillation in the steady states compensates for the lower tracking speed.

The optimization of T_p is also considered. For example, the variable ΔD and T_p depicted in Figs. 20(g) and 22(b) are simultaneously optimized in method No. 9, which results in the MPPT efficiency of 93.9% according to Fig. 21(b). It seems that T_p does not contribute to the MPPT efficiency compared with the methods with fixed T_p such as methods No. 4 and 5 with the efficiencies of 95.1% and 93.9%, respectively. However, the larger T_p than 8.5 ms compensates for the longer settling time due to the bigger ΔD than 4%, according to Fig. 22(b). Therefore, it has a subtle contribution to the MPPT efficiency which leads to more settled inputs for the MPPT algorithm.

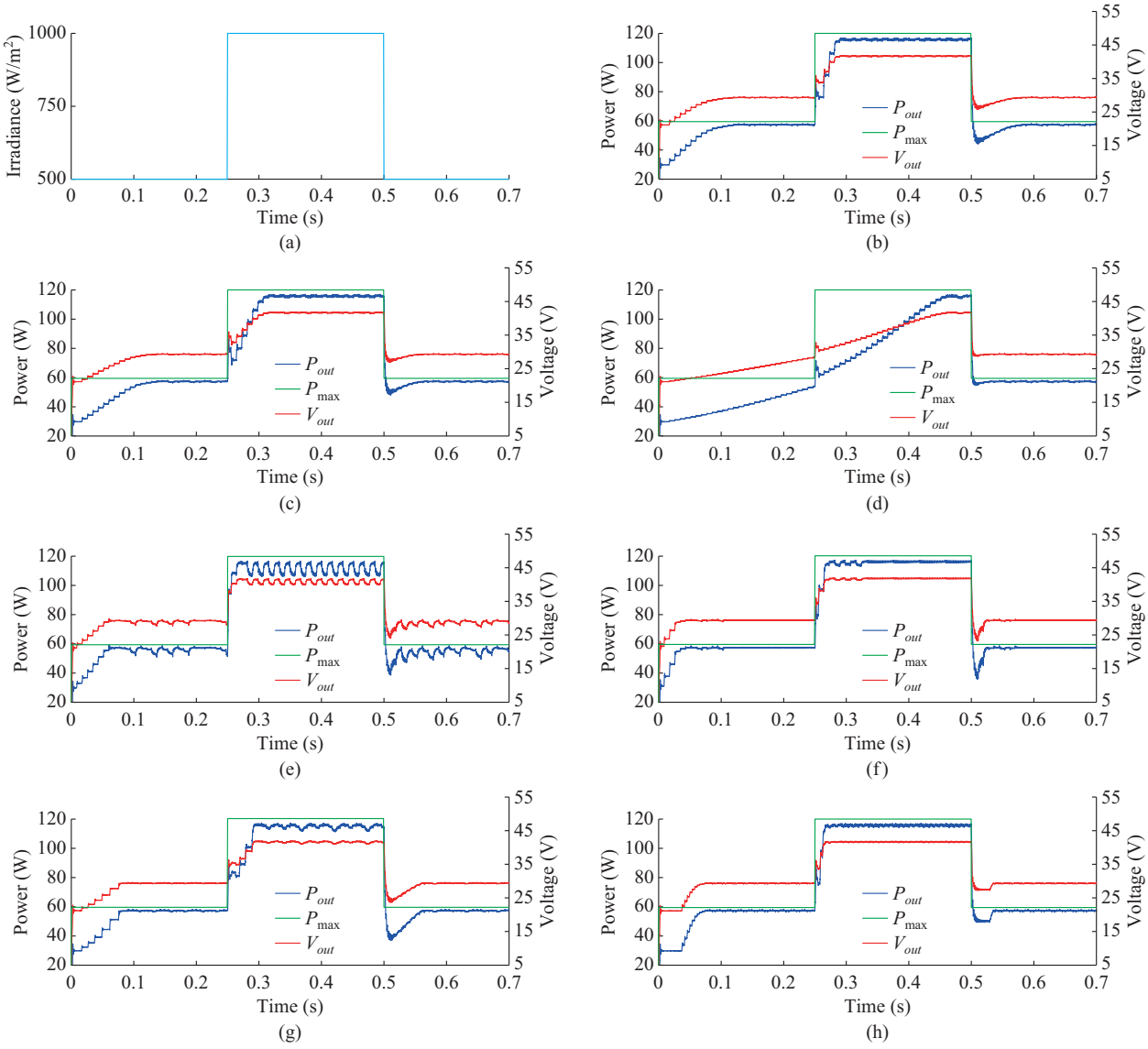

Fig. 19. Output power and voltage of PV systems of Table II. (a) Irradiance profile. (b) Method No. 4. (c) Method No. 5. (d) Method No. 6. (e) Method No. 7. (f) Method No. 8. (g) Method No. 9. (h) Method No. 11.

Moreover, according to Fig. 22(b), T_p converges to around 6 ms in all the steady states. However, as shown in Fig. 22(c), T_p optimized by the system identification technique has different values in each steady state. It means that the optimization of T_p in the transient states differs from that in the steady states. Hence, according to Fig. 22(d) where T_p is adapted for each steady state and is proportional to ΔD in the transient states, method No. 11 complies with this rule. In this way, the three-point oscillation is guaranteed in the steady states.

The output power and voltage of method No. 10 are shown in Fig. 21(c). It is computationally complex compared with the other methods in Table II, which offers distinctive features. Firstly, PRBS injected to the control input of IPC resembles the white noise. Therefore, since PRBS is uncorrelated with the disturbances affecting the PV voltage, the system identification technique has intrinsic noise immunity and copes well with system uncertainties. Secondly, due to the online optimization, the system identification has robustness under different weather conditions during the whole life of PV systems.

The following outcomes are deduced.

1) When ΔD is optimized based on the slope of the *P-V* and *P-D* curves, different scaling factors must be allocated to ΔD.

2) T_p has different behaviors in the steady and transient states, thus each state needs a different optimization method regarding T_p.

3) The zero-oscillation technique greatly improves the MPPT efficiency. However, to suppress the steady-state oscillations successfully, the steady state should firstly reach the three-point oscillation. Moreover, system identification techniques guarantee the three-point oscillation by the online optimization of T_p. Thus, the system identification techniques can be used to improve the reliability of the zero-oscillation method.

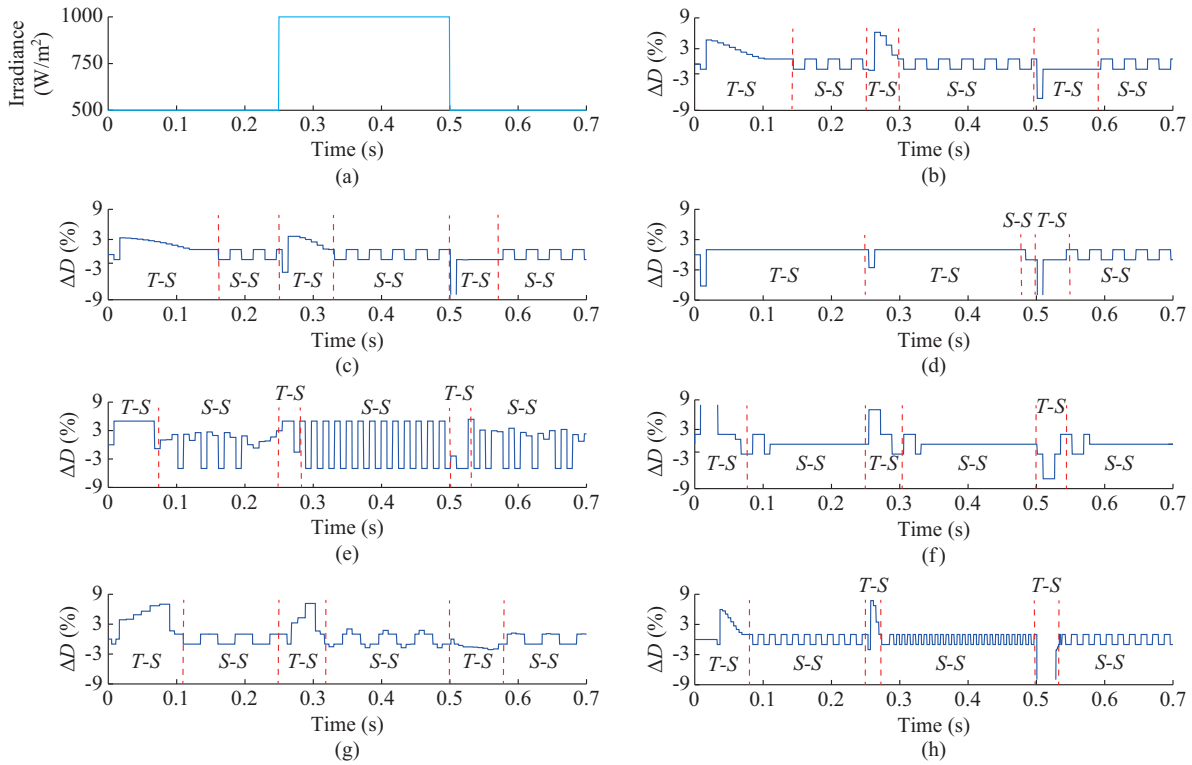

Fig. 20. Variable ΔD in different methods of Table II. (a) Irradiance profile. (b) Method No. 4. (c) Method No. 5. (d) Method No. 6. (e) Method No. 7. (f) Method No. 8. (g) Method No. 9. (h) Method No. 11.

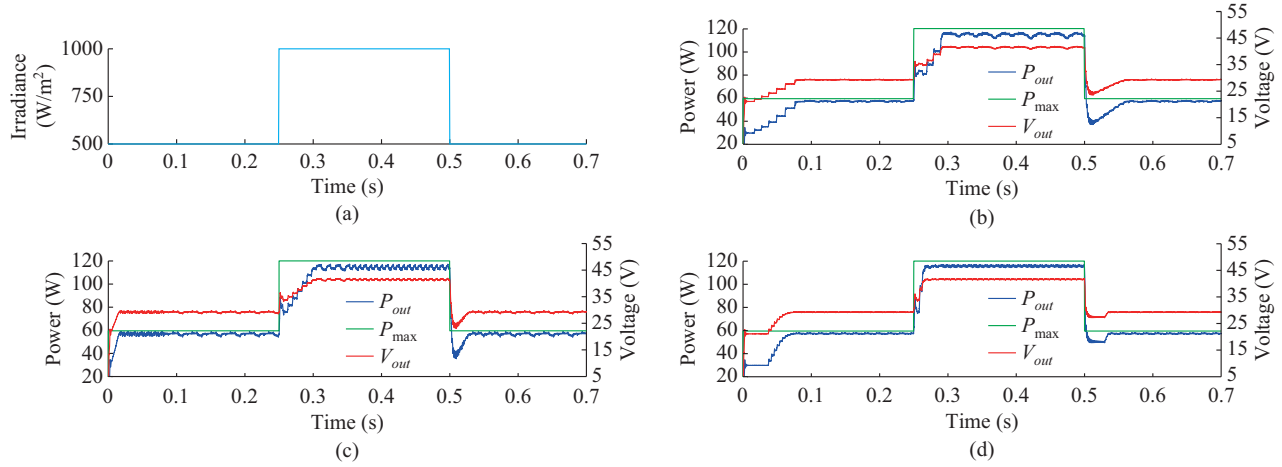

Fig. 21. Output power and voltage of PV systems of Table II. (a) Irradiance profile. (b) Method No. 9. (c) Method No. 10. (d) Method No. 11.

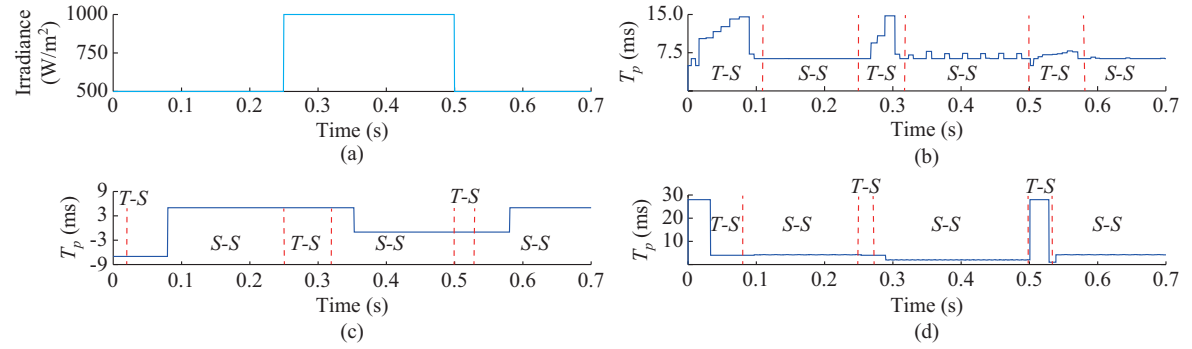

Fig. 22. T_p in different methods of Table II. (a) Irradiance profile. (b) Method No. 9. (c) Method No. 10. (d) Method No. 11.

VII. Conclusion

To achieve a desired tracking speed and efficiency of MPPT, ΔD and T_p should be optimized accordingly. In this paper, various optimization methods of the MPPT parameters are surveyed, classified, simulated, compared, and discussed. With the discussion and comparison based on Table II and Figs. 19-22, the contribution of each optimization method to the MPPT efficiency is quantified, and key features like noise immunity, robustness, and computation effort are investigated. Moreover, this paper sheds light on why steady and transient states need different optimization methods. Besides, subtle contributions of some optimization methods to the MPPT efficiency are revealed. In addition, the possibility of increasing the reliability of the zero-oscillation method by the online system identification techniques is introduced.

References

[1] M. A. M. Ramli, S. Twaha, K. Ishaque *et al*., "A review on maximum power point tracking for photovoltaic systems with and without shading conditions," *Renewable and Sustainable Energy Reviews*, no. 67, pp. 144-159, Jan. 2017.

[2] M. A. Elgendy, B. Zahawi, and D. J. Atkinson, "Operation characteristics of the P&O algorithm at high perturbation frequencies for standalone PV systems," *IEEE Transactions on Energy Conversion*, vol. 30, no. 1, pp. 189-198, Mar. 2015.

[3] M. A. Elgendy, D. J. Atkinson, and B. Zahawi, "Experimental investigation of the incremental conductance maximum power point tracking algorithm at high perturbation rates," *IET Renewable Power Generation*, vol. 10, no. 2, pp. 133-139, Feb. 2016.

[4] K. Sundareswaran, V. V. Kumar, and S. Palani, "Application of a combined particle swarm optimization and perturb and observe method for MPPT in PV systems under partial shading conditions," *Renewable Energy*, vol. 75, pp. 308-317, Mar. 2015.

[5] M. Bahrami, R. Gavagsaz-Ghoachani, M. Zandi *et al*.,"Hybrid maximum power point tracking algorithm with improved dynamic performance," *Renewable Energy*, vol. 130, pp. 982-991, Jan. 2019.

[6] J. Kivimaki, S. Kolesnik, M. Sitbon *et al*., "Design guidelines for multi-loop perturbative maximum power point tracking algorithms," *IEEE Transactions on Power Electronics*, vol. 33, no. 2, pp. 1284-1293, Feb. 2018.

[7] N. Femia, G. Petrone, G. Spagnuolo *et al.*, *Power Electronics and Control Techniques for Maximum Energy Harvesting in Photovoltaic Systems*, 1st ed. Boca Raton: CRC press, 2012, pp. 45-90.

[8] F. Belhachat and C. Larbes, "A review of global maximum power point tracking techniques of photovoltaic system under partial shading conditions," *Renewable and Sustainable Energy Reviews*, vol. 92, pp. 513-553, Sept. 2018.

[9] J. Kivimäki, S. Kolesnik, M. Sitbon *et al*., "Revisited perturbation frequency design guideline for direct fixed-step maximum power point tracking algorithms," *IEEE Transactions on Industrial Electronics*, vol. 64, no. 6, pp. 4601-4609, Jun. 2017.

[10] P. Manganiello, M. Ricco, G. Petrone *et al*., "Optimization of perturbative PV MPPT methods through online system identification," *IEEE Transactions on Industrial Electronics*, vol. 61, no. 12, pp. 6812-6821, Dec. 2014.

[11] M. Shayestegan, "Overview of grid-connected two-stage transformerless inverter design," *Journal of Modern Power Systems and Clean Energy*, vol. 6, no. 4, pp. 642-655, Jul. 2018.

[12] S. B. Kjær, "Evaluation of the hill climbing and the incremental conductance maximum power point trackers for photovoltaic power systems," *IEEE Transactions on Energy Conversion*, vol. 27, no. 4, pp. 922-929, Dec. 2012.

[13] D. G. Montoya, C. A. R. Paja, and G. Petrone, "Design method of the perturb and observe controller parameters for photovoltaic applications," in *Proceedings of IEEE 4th Colombian Workshop on Circuits and Systems (CWCAS)*, Barranquilla, Colombia, Nov. 2012, pp. 1-6.

[14] S. D. Al-Majidi, M. F. Abbod, and H. S. Al-Raweshidy, "A novel maximum power point tracking technique based on fuzzy logic for photovoltaic systems," *International Journal of Hydrogen Energy*, vol. 43, no. 31, pp. 14158-14171, Aug. 2018.

[15] R. Subha and S. Himavathi, "Active power control of a photovoltaic system without energy storage using neural network-based estimator and modified P&O algorithm," *IET Generation, Transmission & Distribution*, vol. 12, no. 4, pp. 927-934, Feb. 2018.

[16] Y. Jiang, J. A. A. Qahouq, and T. A. Haskew, "Adaptive step size with adaptive-perturbation-frequency digital MPPT controller for a single-sensor photovoltaic solar system," *IEEE Transactions on Power Electronics*, vol. 28, no. 7, pp. 3195-3205, Jul. 2013.

[17] Y. Shi, R. Li, Y. Xue *et al*., "High-frequency-link-based grid-tied PV system with small DC-link capacitor and low-frequency ripple-free maximum power point tracking," *IEEE Transactions on Power Electronics*, vol. 31, no. 1, pp. 328-339, Jan. 2016.

[18] A. Pandey, N. Dasgupta, and A. K. Mukerjee, "High-performance algorithms for drift avoidance and fast tracking in solar MPPT system," *IEEE Transactions on Energy Conversion*, vol. 23, no. 2, pp. 681-689, Jun. 2008.

[19] N. E. Zakzouk, M. A. Elsaharty, A. K. Abdelsalam *et al*., "Improved performance low-cost incremental conductance PV MPPT technique," *IET Renewable Power Generation*, vol. 10, no. 4, pp. 561-574, Mar. 2016.

[20] S. Messalti, A. Harrag, and A. Loukriz, "A new variable step size neural networks MPPT controller: review, simulation and hardware implementation," *Renewable and Sustainable Energy Reviews*, vol. 68, no. 1, pp. 221-233, Feb. 2017.

[21] C. C. Hua, Y. H. Fang, and W. T. Chen, "Hybrid maximum power point tracking method with variable step size for photovoltaic systems," *IET Renewable Power Generation*, vol. 10, no. 2, pp. 127-132, Feb. 2016.

[22] R. Faraji, A. Rouholamini, H. R. Naji *et al*., "FPGA-based real time incremental conductance maximum power point tracking controller for photovoltaic systems," *IET Power Electronics*, vol. 7, no. 5, pp. 1294-1304, May 2014.

[23] A. I. M. Ali, A. S. Mohamed, and E. E. M. Mohamed, "Modified efficient perturb and observe maximum power point tracking technique for grid-tied PV system," *International Journal of Electrical Power & Energy Systems*, vol. 99, pp. 192-202, Jul. 2018.

[24] Q. Mei, M. Shan, L. Liu *et al*., "A novel improved variable step-size incremental-resistance MPPT method for PV systems," *IEEE Transactions on Industrial Electronics*, vol. 58, no. 6, pp. 2427-2434, Aug. 2011.

[25] M. Killi and S. Samanta, "An adaptive voltage-sensor-based MPPT for photovoltaic systems with SEPIC converter including steady-state and drift analysis," *IEEE Transactions on Industrial Electronics*, vol. 62, no. 12, pp. 7609-7619, Jul. 2015.

[26] A. Loukriz, M. Haddadi, and S. Messalti, "Simulation and experimental design of a new advanced variable step size incremental conductance MPPT algorithm for PV systems," *ISA Transactions*, vol. 62, pp. 30-38, May 2016.

[27] L. Peng, S. Zheng, X. Chai *et al*., "A novel tangent error maximum power point tracking algorithm for photovoltaic system under fast multi-changing solar irradiances," *Applied Energy*, vol. 210, pp. 303-316, Jan. 2018.

[28] Y. T. Chen, Y. C. Jhang, and R. H. Liang, "A fuzzy-logic based auto-scaling variable step-size MPPT method for PV systems," *Solar Energy*, vol. 126, pp. 53-63, Mar. 2016.

[29] S. M. R. Tousi, M. H. Moradi, N. S. Basir *et al*., "A function-based maximum power point tracking method for photovoltaic systems," *IEEE Transactions on Power Electronics*, vol. 31, no. 3, pp. 2120-2128, Mar. 2016.

[30] A. Ahmed, L. Ran, S. Moon *et al*., "A fast PV power tracking control algorithm with reduced power mode," *IEEE Transactions on Energy Conversion*, vol. 28, no. 3, pp. 565-575, Sept. 2013.

[31] O. Khan and W. Xiao, "Integration of start-stop mechanism to improve maximum power point tracking performance in steady state," *IEEE Transactions on Industrial Electronics*, vol. 63, no. 10, pp. 6126-6135, Oct. 2016.

[32] J. Ahmed and Z. Salam, "An enhanced adaptive P&O MPPT for fast and efficient tracking under varying environmental conditions," *IEEE Transactions on Sustainable Energy*, vol. 9, no. 3, pp. 1487-1496, Jul. 2018.

[33] J. Ahmed and Z. Salam, "A modified P&O maximum power point tracking method with reduced steady-state oscillation and improved tracking efficiency," *IEEE Transactions on Sustainable Energy*, vol. 7, no. 4, pp. 1506-1515, May 2016.

[34] T. H. Kwan and X. Wu, "An adaptive scale factor based MPPT algorithm for changing solar irradiation levels in outer space," *Acta Astro-*

nautica, vol. 132, pp. 33-42, Mar. 2017.
[35] X. Li, H. Wen, L. Jiang *et al*., "An improved MPPT method for PV system with fast-converging speed and zero oscillation," *IEEE Transactions on Industry Applications*, vol. 52, no. 6, pp. 5051-5064, Dec. 2016.
[36] F. Paz and M. Ordonez, "Zero oscillation and irradiance slope tracking for photovoltaic MPPT," *IEEE Transactions on Industrial Electronics*, vol. 61, no. 11, pp. 6138-6147, Nov. 2014.
[37] H. Bounechba, A. Bouzid, H. Snani *et al*., "Real time simulation of MPPT algorithms for PV energy system," *International Journal of Electrical Power & Energy Systems*, vol. 83, pp. 67-78, Dec. 2016.
[38] A. Harrag and S. Messalti, "Variable step size modified P&O MPPT algorithm using GA-based hybrid offline/online PID controller," *Renewable and Sustainable Energy Reviews*, vol. 49, pp. 1247-1260, Sept. 2015.
[39] A. K. Abdelsalam, A. M. Massoud, S. Ahmed *et al*., "High-performance adaptive perturb and observe MPPT technique for photovoltaic-based microgrids," *IEEE Transactions on Power Electronics*, vol. 26, no. 4, pp. 1010-1021, Apr. 2011.
[40] D. Kler, K. P. S. Rana, and V. Kumar, "A nonlinear PID controller based novel maximum power point tracker for PV systems," *Journal of the Franklin Institute*, vol. 335, no. 16, pp. 7827-7864, Nov. 2018.
[41] M. Sitbon, S. Lineykin, S. Schacham *et al*., "Online dynamic conductance estimation based maximum power point tracking of photovoltaic generators," *Energy Conversion and Management*, vol. 166, pp. 687-696, Jun. 2018.
[42] C. Huang, L. Wang, R. S. C. Yeung *et al*., "A prediction model-guided jaya algorithm for the PV system maximum power point tracking," *IEEE Transactions on Sustainable Energy*, vol. 9, no. 1, pp. 45-55, Jan. 2018.
[43] M. A. Ghasemi, A. Ramyar, and H. Iman-Eini, "MPPT method for PV systems under partially shaded conditions by approximating *I-V* curve," *IEEE Transactions on Industrial Electronics*, vol. 65, no. 5, pp. 3966-3975, Oct. 2018.
[44] D. G. Montoya, C. A. Ramos-Paja, and R. Giral, "Improved design of sliding-mode controllers based on the requirements of MPPT techniques," *IEEE Transactions on Power Electronics*, vol. 31, no. 1, pp. 235-247, Jan. 2016.
[45] M. Shirazi, J. Morroni, A. Dolgov *et al*., "Integration of frequency response measurement capabilities in digital controllers for DC-DC converters," *IEEE Transactions on Power Electronics*, vol. 23, no. 5, pp. 2524-2535, Sept. 2008.
[46] T. Roinila, T. Helin, M. Vilkko *et al*., "Circular correlation based identification of switching power converter with uncertainty analysis using fuzzy density approach," *Simulation Modelling Practice and Theory*, vol. 17, no. 6, pp. 1043-1058, Jul. 2009.
[47] A. Barkley and E. Santi, "Improved online identification of a DC-DC converter and its control loop gain using cross-correlation methods," *IEEE Transactions on Power Electronics*, vol. 24, no. 8, pp. 2021-2031, Aug. 2009.
[48] M. Algreer, M. Armstrong, and D. Giaouris, "Active online system identification of switch mode DC-DC power converter based on efficient recursive DCD-IIR adaptive filter," *IEEE Transactions on Power Electronics*, vol. 27, no. 11, pp. 4425-4435, Nov. 2012.
[49] M. Ricco, P. Manganiello, G. Petrone *et al*., "FPGA-based implementation of an adaptive P&O MPPT controller for PV applications," in *Proceedings of IEEE 23rd International Symposium on Industrial Electronics*, Istanbul, Turkey, Jun. 2014, pp. 1876-1881.
[50] M. Ricco, P. Manganiello, E. Monmasson *et al*., "FPGA-based implementation of dual Kalman filter for PV MPPT applications," *IEEE Transactions on Industrial Informatics*, vol. 13, no. 1, pp. 176-185, Feb. 2017.
[51] P. Manganiello, M. Ricco, G. Petrone *et al*., "Dual-Kalman-filter-based identification and real-time optimization of PV systems," *IEEE Transactions on Industrial Electronics*, vol. 62, no. 11, pp. 7266-7275, Nov. 2015.
[52] J. Dadkhah and M. Niroomand, "Real-time MPPT optimization of PV systems by means of DCD-RLS based identification," *IEEE Transactions on Sustainable Energy*, vol. 10, no. 4, pp. 2114-2122, Oct. 2019.
[53] J. Dadkhah and M. Niroomand, "Optimization of MPPT in both steady and transient states through variable parameters," in *Proceedings of Iranian Conference on Electrical Engineering (ICEE)*, Mashhad, Iran, May 2018, pp. 1132-1137.

Jalal Dadkhah received the B.S. degree in electronic engineering from Islamic Azad University, Isfahan, Iran, in 2014, and the M.S. degree in electronic engineering from University of Isfahan, Isfahan, Iran, in 2018. He is currently working toward the Ph.D. degree in power electronics at the University of Manitoba, Winnipeg, Canada. His research interests include grid-connected power converters and renewable energy applications.

Mehdi Niroomand received the B.S., M.S., and Ph.D. degrees in electrical engineering from Isfahan University of Technology (IUT), Isfahan, Iran, in 2001, 2004, and 2010, respectively. Since 2010, he has been with the Department of Electrical Engineering, University of Isfahan, Isfahan, Iran, where he is currently an Associate Professor. His research interests include power electronics, PV systems, switching power supplies and control in power electronics.